Contents lists available at ScienceDirect

Biosensors and Bioelectronics

Label-free enumeration of colorectal cancer cells from lymphocytes performed at a high cell-loading density by using interdigitated ring-array microelectrodes

Xiaoxing Xing [a], Randy Y.C. Poon [b], Cesar S.C. Wong [c], Levent Yobas [a,*]

[a] Department of Electronic and Computer Engineering, The Hong Kong University of Science and Technology, Clear Water Bay, Kowloon, Hong Kong Special Administrative Region
[b] Division of Life Science, The Hong Kong University of Science and Technology, Clear Water Bay, Kowloon, Hong Kong Special Administrative Region
[c] Department of Health Technology and Informatics, Faculty of Health and Social Sciences, Hong Kong Polytechnic University, Hung Hom, Kowloon, Hong Kong Special Administrative Region

A B S T R A C T

We report the label-free enumeration of human colorectal-carcinoma cells from blood lymphocytes by using interdigitated ring-array microelectrodes; this enumeration was based on the dielectrophoretic selection of cells. Because of the novel design of the device, a continuous flow of cells is uniformly distributed into parallel streams through 300 rings ($\sim 40\,\mu m$ in diameter each) that are integrated into the electrode digits. Using this array, 82% of cancer cells were recovered and 99% of blood lymphocytes were removed. Most of the cancer cells recovered were viable (94%) and could be cultivated for > 8 days, during which period they retained their normal cell morphology and proliferation rates. The recovery rate correlated closely with cancer-cell loadings in spiked samples and this relationship was linear over a range of at least 2 orders of magnitude. Importantly, because of the 3D structure of the rings, these results were obtained at a high cell-loading concentration (10^7 cells/mL). The rings could be further optimized for use in accurate label-free identification and measurement of circulating tumor cells in cancer research and disease management.

© 2014 Elsevier B.V. All rights reserved.

1. Introduction

Clinically occult metastases are responsible for the vast majority of deaths in patients with solid tumors (Steeg, 2006). Tumor cells that acquire the ability to penetrate the lymphatic system and blood vessels enter the bloodstream and potentially infiltrate distant organs. Such tumor-derived epithelial cells are referred to as circulating tumor cells (CTCs) (Gupta and Massague, 2006). The process by which primary tumor sites shed CTCs into the bloodstream is not well understood. Thus, phenotypic and molecular characterization of viable CTCs isolated from the blood of metastatic-cancer patients could greatly help in enhancing the current understanding of metastases and in the identification of therapeutic targets. Moreover, recent studies suggest that the viable CTC count in peripheral blood is directly linked to cancer progression (Cristofanilli et al., 2004). Therefore, enumerating CTCs could become an approach that is used instead of invasive

biopsies for the purpose of stratifying patients for adjuvant therapies and increasing the follow-up frequency during the course of the treatments.

Because CTCs are present in peripheral blood at extremely low abundance (a few to hundred CTCs are present among 10^9 red cells/mL and 10^6 white cells/mL blood), isolating CTCs is a needle-in-a-haystack challenge. The classical techniques used to isolate CTCs to date, including filtration (Vona et al., 2000), density-gradient centrifugation (Rosenberg et al., 2002), and immunomagnetic enrichment (Wong et al., 1995), have been determined to be inadequately specific and sensitive, and the task calls for the development of a technology that can be used to screen samples rapidly and deterministically at single-cell resolution. Microfluidics has demonstrated this capability in sorting and detecting cells in controlled microenvironments (Davis et al., 2006; Huang et al., 2004).

In several microfluidic approaches, affinity-based protocols are employed by using monoclonal antibodies (mAbs) specific to antigenic integral-membrane proteins such as the epithelial-cell-adhesion molecule (EpCAM) (Adams et al., 2008; Nagrath et al., 2007). However, antigen labeling might not be highly effective

* Corresponding author. Tel.: +852 2358 7068; fax: +852 2358 1485.
E-mail address: eelyobas@ust.hk (L. Yobas).

because the expression level of antigens varies from cell to cell depending on the cell stage and the type of tumor. For instance, EpCAM is not expressed in non-epithelial solid malignancies and is downregulated in malignant epithelial cells undergoing epithelial-to-mesenchymal transition (EMT) (Thiery and Sleeman, 2006). Moreover, CTC enrichment based on surface markers is hampered by the lack of a universal tumor marker that is independent of tumor type and also by the heterogeneity of cells within the same tumor tissue. Because of these drawbacks, attempts have been made to develop methods that are independent of antigen-based interactions (Tan et al., 2009, 2010).

Dielectrophoresis (DEP) has been arguably the most widely used antigen-independent method of isolating unmodified viable tumor cells since the seminal work of Gascoyne et al. (1992). By using a flat flow chamber in which thin-film interdigitated electrodes line the chamber floor, Becker and coworkers harvested viable human leukemia HL-60 cells (Becker et al., 1994) and cells of the metastatic breast-cancer cell line MDA231 (Becker et al., 1995) from whole blood. Using this technique, 100% efficiency was achieved in purging breast-cancer cells from blood at tumor-cell to normal-cell ratios as low as $1:3 \times 10^5$ (Gascoyne et al., 1997). Moreover, a highly selective method of cell discrimination at high medium conductivities was developed by combining DEP with field-flow fractionation (DEP/FFF) (Markx et al., 1997), and the performance of the method was demonstrated by isolating HL-60 cells from peripheral blood mononuclear (PBMN) cells (Huang et al., 1997) and breast-cancer MDA-435 cells from normal blood cells (Yang et al., 1999), and further by separating breast-cancer cells from normal T-lymphocytes and CD34+ hematopoietic stem cells (Huang et al., 1999; Wang et al., 2000). This batch technique was later scaled up to increase the array size to enable the handling of considerably increased numbers of cells, and the technique was tested in the isolation of various types of breast-cancer cell lines from mixtures containing up to 30×10^6 PBMN cells (Gascoyne et al., 2009). The approach led to the development of electrosmear, a cytological slide-preparation method in which cells exhibiting distinct dielectric properties were localized into separate zones, tumor cells in a low-frequency zone, and blood cells in a high-frequency zone (Das et al., 2005). Electrosmear was also used in needle biopsies to isolate tumor cells from other cell types (Cristofanilli et al., 2008). DEP/FFF was recently upgraded to a continuous-mode operation whereby tumor cells can be continually harvested upon isolation by skimming from the flow chamber in which the nucleated cells are slowly injected and deionized by diffusion (Gupta et al., 2012; Shim et al., 2013b).

Numerous studies have shown that DEP can be used to isolate tumor cells from a mixture of distinct types of cells; the designs used in these studies have ranged from a simple assembly of bulk needle electrodes (Broche et al., 2007) to thin-film surface-patterned electrodes that were interdigitated (Alazzam et al., 2011), castellated (Sabuncu et al., 2010), triangular (Alshareef et al., 2013; Ling et al., 2012; Yang et al., 2010), circular (Cheng et al., 1998; Huang et al., 2002; Jen and Chang, 2011), or in 3D-asymmetric shapes (An et al., 2009; Park et al., 2005). Tumor cells have also been isolated using variants of DEP such as travelling-wave DEP (Cen et al., 2004; van den Driesche et al., 2012), electrorotation (Cen et al., 2004), guided DEP (Kostner et al., 2010), curve-induced DEP (Zhu and Xuan, 2011), dc-DEP (Kang et al., 2008; Sun et al., 2012), contactless DEP (cDEP) (Salmanzadeh et al., 2012a, 2012b), and multi-frequency DEP (Valero et al., 2010), and further by means of DEP used in conjunction with other cell-separation modalities including multi-orifice flow fractionation (MOFF) (Moon et al., 2011) or magnetophoresis (Jung et al., 2011). These studies were conducted by mainly employing cancer cell-line models of breast cancer (Cristofanilli et al., 2008; Das et al., 2005; Gascoyne et al., 2009; Huang et al., 1999; Wang et al., 2000),

oral cancer (Broche et al., 2007), melanoma (Sabuncu et al., 2010), leukemia (Becker et al., 1994; Huang et al., 1997), lymphoma and myeloma (Cen et al., 2004), and cervical (Cheng et al., 1998), ovarian (Salmanzadeh et al., 2012a), prostate (Salmanzadeh et al., 2012b), and colorectal cancers (Alshareef et al., 2013; Yang et al., 2010). A recent survey has further shown that DEP can be used to discriminate all types of tumor cells listed in the NCI-60 panel and PBMN cells (Shim et al., 2013a). These pioneering studies and other studies that established DEP as a potential tumor cell-isolation technique have been described at length in recent reviews (Arya et al., 2013; Chen et al., 2012; Hyun and Jung, 2013).

Previous DEP designs offer both advantages and disadvantages. The surface electrodes are convenient to fabricate but project a force field that is too limited to influence cells at a distance. The effectiveness of field penetration into the sample can be enhanced using 3D electrodes, but this increases fabrication complexity. The use of insulator- or dc-DEP resolves such concerns by delegating the spatially effective field to externally placed wire electrodes, but
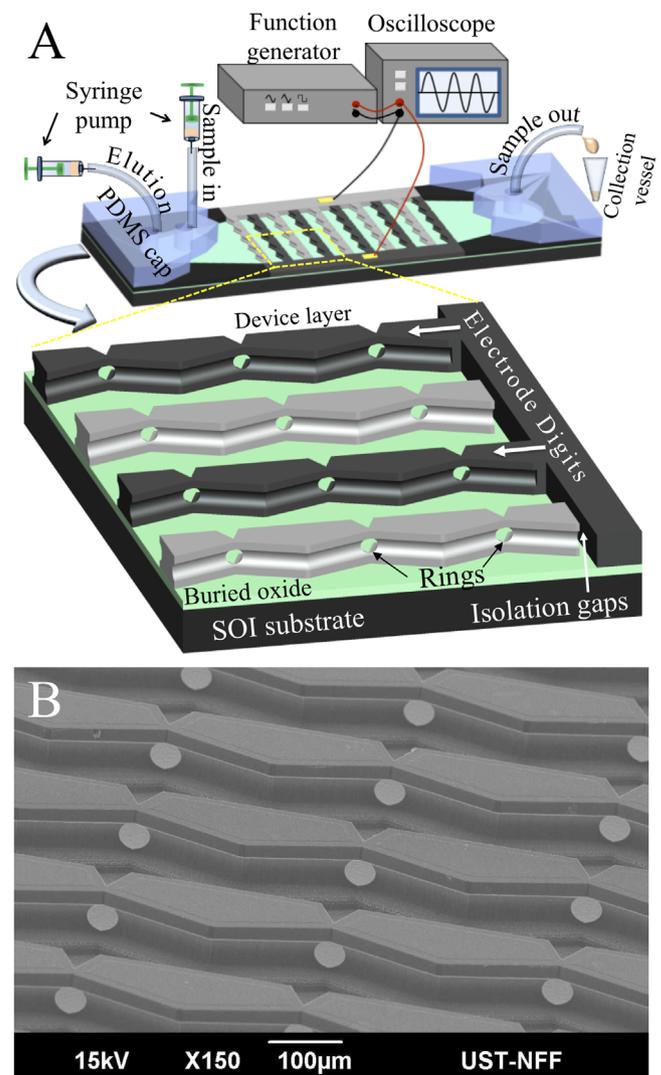
Fig. 1. (A) A 3D rendering of the overall design and the experimental setup. The polydimethylsiloxane (PDMS) cap is partially drawn to reveal the electrode structure that is further detailed in a close-up view of the segment demarcated by the dashed lines (in the lower panel, rotated 90°). The chamber is supplied by 2 adjacent inlet ports that feature separate syringe pumps dedicated to the cell suspension (the sample) and the elution buffer, whereas the eluent is collected from a single outlet port. The 3D silicon electrodes are activated by applying ac voltage to the pads. (B) SEM image of a representative device section that further reveals the electrode structure.

this limits the bandwidth because high activation voltages are required to compensate for the distance between electrodes. In cDEP, contact is avoided between the sample and the externally placed electrodes and the voltage requirement is lowered to some extent, and thus cDEP allows for increased activation frequencies.

Recently, we introduced a novel 3D DEP design that is simple to fabricate and has the capacity to process particles in parallel streams flowing through an array of coaxial ring electrodes (Xing et al., 2013). The rings within each alternating row are interconnected and form a set of electrode digits, and together these constitute a unique design of interdigitated 3D array electrodes that feature a built-in flow chamber in between (Fig. 1). Thus, the structure projects a highly effective force field across the entire flow chamber, unlike in the case of a quasi-2D design. We previously addressed the fabrication aspects of the design and demonstrated its functionality in the manipulation and isolation of polystyrene microspheres based purely on microsphere size (Xing et al., 2013). Here, we report for the first time that this design can be used effectively in an application that is of biological significance: label-free, dielectric signature-based enumeration of human colorectal-cancer cells from lymphocytes, performed at a high cell-loading density of $\sim 10^7$ cells/mL. This is in contrast with many of the state-of-the-art microfluidic DEP devices because the cell-loading density of those devices is limited and their cell-isolation efficiency and purity deteriorate before a cell-loading density of 10^6 cells/mL can be reached (Gascoyne et al., 2009). This is mainly because the electrode area in these mostly quasi-2D designs is limited and because the dipole–dipole interactions between cells perturb their DEP response and lead to cell aggregation. Through systematic experimentation, we demonstrate that our device featuring the novel design can be used to selectively capture and recover cancer cells and concomitantly remove nucleated blood cells at set values of flow rate and activation frequency. We also show that the recovered cancer cells are viable and can be cultivated for further analysis.

2. Theory

A brief introduction to the theory of DEP is presented in Supplementary information.

3. Material and methods

3.1. Cells and reagents

Peripheral blood (~ 9 mL) was drawn from healthy volunteers into vacuum tubes coated with EDTA anticoagulant (VACUETTE® EDTA Tubes, Greiner Bio-One). The blood was diluted at a 1:1 ratio using phosphate-buffered saline (PBS) solution (containing, per liter, 8 g NaCl, 0.2 g KCl, 1.44 g Na_2HPO_4, and 0.24 g KH_2PO_4; pH 7.4) and layered onto Ficoll-Paque PLUS (GE Healthcare Lifescience, Inc) in a 50-mL BD falcon conical tube (BD Falcon™), and then centrifuged for 30 min at 400g at 20 °C (Megafuge 1.0 R). The PBMN cells that mainly comprised lymphocytes were then transferred into a 15-mL polystyrene conical centrifuge tube (BD Falcon™) and washed with 6 mL PBS for 10 min at $100 \times g$ to remove blood platelets. The cell pellet obtained was suspended in DEP buffer (300 mM D-Mannitol, conductivity tuned to 100 μS/cm using PBS) in a 1.5-mL conical tube at a final cell density of 10^7/mL; the conductivity of the DEP buffer was measured with a conductivity meter (Mettler-Toledo, SevenGo Duo pro).

HCT116 cells (human colorectal-carcinoma cells, ATCC) were cultured in McCoy's 5a (modified) medium supplemented with 10% fetal bovine serum (FBS) and incubated in a 5% CO_2

environment at 37 °C. Before each experiment, cells were washed with PBS and then detached from culture dishes by treating them with trypsin–EDTA; the detached cells were suspended in the original culture medium. HCT116 cells were pre-stained with 2 μg/mL Calcein-AM (Life Technologies, Inc.), incubated for 20 min at 37 °C in the dark, and then washed with DEP buffer twice at 100g for 5 min. Next, the cells were spiked into lymphocyte suspensions at a ratio of around 1:200, and the final lymphocyte density was set at 10^7 cells/mL. In the experiments performed to visualize the separation of cancer cells from lymphocytes within the device, lymphocytes were stained 2 μg/mL of the nucleic-acid dye Hoechst 33342 (Life Technologies, Inc.) and incubated for 20 min at 37 °C in the dark.

3.2. Fabrication

The fabrication process is described briefly in the Supplementary information. A more detailed description is presented in our earlier reports on the process (Xing et al., 2013; Yobas et al., 2005).

3.3. Experiments

Before each experiment, all materials were sterilized. Buffer solutions were passed through a 0.22-μm membrane filter. All the syringes, filters, pipette tips, and conical centrifuge tubes were UV-irradiated for 10 min. The chip and tubing (Tygon) were disinfected using 70% ethanol and then rinsed with DI water. After sterilization, to minimize cell adhesion, the chip was coated with 5% BSA in DEP buffer for 30 min and then preconditioned using the same buffer. A sine-wave voltage signal was applied on the electrodes from a function generator (Tektronix CFG250) while being monitored on an oscilloscope (Tektronix TDS 2012C). The 2 inlet ports were inserted together with the tubings that were connected to 1-mL syringes (BD Tuberculin); these syringes were independently controlled by dedicated syringe pumps (Harvard Apparatus) to inject the sample and eluate buffer (Fig. 1). Each experiment was initiated by activating the electrodes and then the sample-injection pump. After depleting the entire sample, the electrodes were switched off and the eluate pump was turned on to recover the enriched cells into a vessel at a rate of 3 mL/h. The cells eluted were transferred onto a glass slide and enumerated under an epifluorescence microscope (Nikon Eclipse, FN1) equipped with a CCD camera (RT3Mono, SPOT). The performance of the device was evaluated based on the rate of cancer-cell recovery and the efficiency of blood–lymphocyte removal. The recovery rate was defined as the percentage of cancer cells successfully recovered using the device with respect to the total number of cells initially spiked into the input sample. Similarly, the removal efficiency was defined as the fraction of lymphocytes discarded from the recovered sample in relation to their total count in the input sample. We manually counted in triplicate all cells in 20-μL eluted samples that were transferred onto a glass slide, mounted with a cover slip, and then placed under the microscope.

3.4. Cell viability

To assess viability, the recovered cells were stained with 50 μg/mL propidium iodide (PI, Sigma-Aldrich) and incubated for 20 min at room temperature in the dark. The percentage of viable cells was derived by excluding the cells that were permeant to PI. The recovered cells were also reseeded and cultured in 96-well plates (~ 500 cells/well) and their growth potential was compared with that of control cells that had not been passed through the device. To each well, 200 μL of culture medium (McCoy's 5a supplemented with 10% FBS) was added and the cells were

incubated in a 5% CO_2 environment at 37 °C for up to 8 days. Each day, cells in a selected well from the control and test groups were harvested using trypsin–EDTA and counted. To the remaining wells, 200 µL of fresh culture medium was added daily and the propagation of cells was imaged under an inverted microscope (Nikon TE2000E-PFS) mounted with a CCD camera (Spot Boost EMCCD, Diagnostic Instruments).

4. Results and discussion

4.1. Design and simulation

Briefly, the device design includes an interdigitated comb structure—composed of 75-µm-thick single crystal-doped silicon —that serves as both the electrodes and the walls of the active flow chamber. The electrode digits (15 pairs) display a characteristic layout featuring a set of alternatingly arranged narrow (20 µm) and wide (140 µm) segments along the digit length (~3 mm). Beneath each narrow segment lies a round lateral opening (the ring) that is coaxially aligned with the corresponding rings in all the other digits for the purpose of defining an orthogonal flow path. The rings are nearly identical in size and feature a nominal diameter of 40 µm, which is large enough to allow passage of most blood cells and other circulating cells. Each digit containing 10 uniformly spaced rings contributes to a total of 300 rings across the device. Consequently, an input stream of cells gets divided equally into 10 parallel streams inside a large flow chamber (3 mm wide, 9 mm long) and exposed to an effective DEP force field through the coaxial ring electrodes. This facilitates the use of a high cell-loading density (10^7 cells/mL) and still supports the high cell-isolation efficiency attained, as shown herein. The design is further detailed in Fig. S1 in the Supplementary Information.

Fig. 2 shows the simulation results obtained using COMSOL Multiphysics Software v3.5 (Comsol Inc., MA). After specifying the electrical boundary conditions at $\pm 10V_p$ 100 kHz and the complex conductivity values $\sigma^* = \sigma + j\omega\varepsilon$ at the device domains accordingly ($\sigma = 10^5 \, S/m$ and $\varepsilon = 11.7$ at the electrodes, whereas $\sigma = 100 \, \mu S/cm$ and $\varepsilon = 80$ at the buffer), the Laplace equation $\nabla(\sigma^* \cdot \nabla\phi) = 0$ was solved for the potential distribution ϕ. Subsequently, the field $\vec{E} = -\vec{\nabla}\phi$ and the gradient of the field squared $\vec{\nabla}(\vec{E} \cdot \vec{E})$ were computed. The Navier–Stokes equation was solved for obtaining the flow-velocity field under the assumptions of incompressible laminar flow and no slippage. The fluid viscosity and density were specified as 10^{-3} Pa s and 10^3 kg/m^3, respectively. The flow boundary conditions were such that the inlet flow was set at a constant speed of 370 µm/s, which corresponded to the highest flow rate used in experiments (0.3 mL/h) and the outlet was set to no viscous stress.

The $\vec{\nabla}(\vec{E} \cdot \vec{E})$ and the flow-velocity profile reflect the DEP force and hydrodynamic drag exerted on the cells, respectively, given their volume and Claussius–Mossotti factor (real part). The range of values obtained here (Fig. 2A and B) is comparable to those reported for the effective trapping of cells or cell-like particles under positive DEP (pDEP) in previous designs (Salmanzadeh et al., 2012b). The cells passing through the rings experience high shear (Fig. 2C), but this lasts for only a short period (a fraction of a second) and is at a magnitude sufficiently below the cell-lysis limit (5000 1/s). Fig. 2D shows the flow-velocity profile normalized with respect to the inlet velocity (370 µm/s) along an axis passing through the ring centers. As expected, the flow-velocity magnitude peaks inside the rings and dips between the rings. By contrast, the $\vec{\nabla}(\vec{E} \cdot \vec{E})$ profile, also plotted in Fig. 2D, suggests that the DEP force field reaches minima inside the rings and maxima immediately before and after the
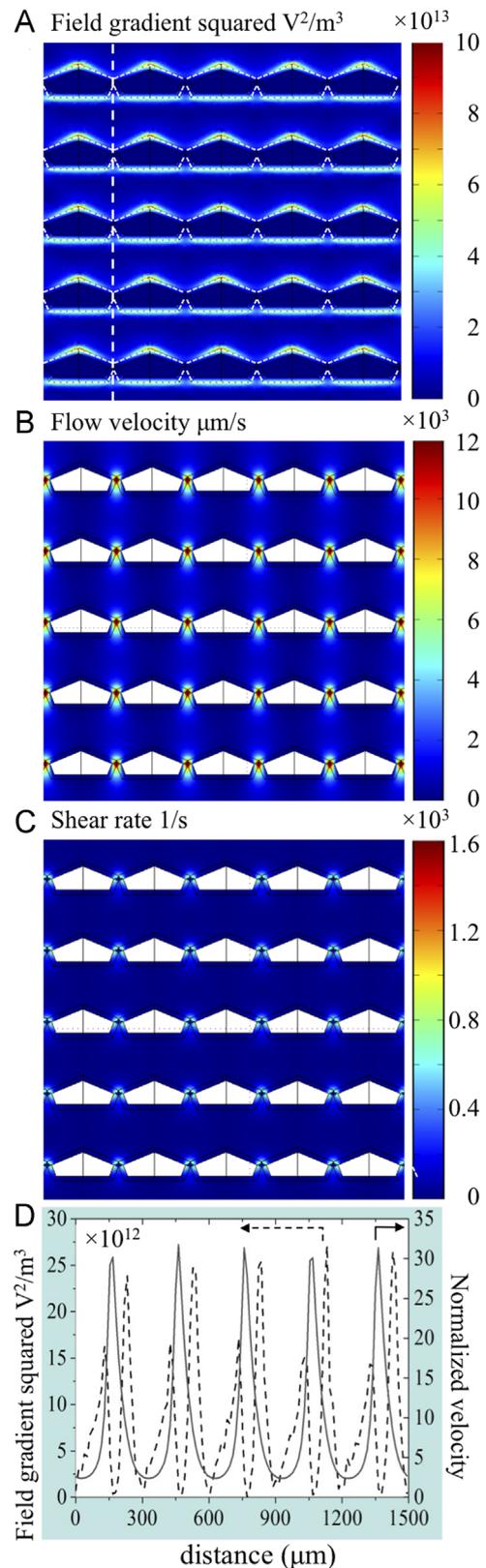
Fig. 2. The results of 3D numerical analyses obtained for a representative device area. (A)–(C) Surface plots across the flow chamber on the horizontal mid-plane. (D) Line plots along the vertical dashed line through the rings in (A). The flow direction is from top to bottom. Simulation conditions and further details were as presented in the text.

rings. The force exerted on cells at a ring exit is slightly greater than that at the ring entrance. This steep field gradient on the sharp-angle side of the ring was generated as a result of the

sudden change in the electrode profile, and this is unlike the more gradual variation that occurs on the opposite side.

4.2. Cell separation

Initial cell experiments were performed on the device by using either human colorectal-cancer cells (HCT116) or lymphocytes isolated from whole blood. Our goal was to evaluate the crossover frequencies of the cells in the suspension buffer under stagnant conditions. Mammalian cells suspended in a buffer featuring a conductivity of 100 μS/cm reportedly exhibit crossover frequencies ranging up to ~100 kHz (Salmanzadeh et al., 2012a). Thus, we scanned the activation gradually from 1 to 500 kHz at a magnitude of ±10 V_p. Cells responded to DEP and showed clear signs of transition from negative to positive DEP near 25 and 60 kHz in the case of the cancer cells and blood cells, respectively. These are slightly below the recently reported values measured using the technique DEP–FFF: around 35 kHz in the case of HCT116 cells and >80 kHz in the case of nucleated blood cells (Shim et al., 2013a). The discrepancy could be explained by the distinct conductivity values of the suspension buffers (300 versus 100 μS/cm) because the crossover frequency tends to increase when the conductivity of the suspension medium is raised (Kirby, 2010).

After identifying the crossover frequencies, we focused on evaluating the conditions required for effectively separating cells through the device. Test samples were prepared that contained the isolated lymphocytes at a density of 10^7 cells/mL and were spiked with HCT116 cells at a ratio of one cancer cell per 200 blood cells; these samples were injected into the device at flow rates of 0.1, 0.2, and 0.3 mL/h. For activating DEP, we selected 4 frequency test points, 35, 45, 65, and 100 kHz, which are all above the characteristic crossover frequency of cancer cells; these frequencies were selected so as to draw the cells toward the electrodes and retain them against the flow under pDEP. The latter 2 points exceeded the crossover frequency of blood cells but were included despite the risk of capturing blood cells because cancer cells can be retained effectively at high frequencies, whereas blood cells facing a weak force field are likely to be swept away by the drag force. The results shown in Fig. 3 confirm this prediction: the representative images reveal the effective trapping of most cancer cells (green) by the electrodes activated at ±10V_p 100 kHz against a stream at a flow rate of 0.2 mL/h. Moreover, DEP did not noticeably affect the blood cells and these cells thus maintained their pre-activation flow patterns. This is further demonstrated in the movie included in the Supplementary information.

Supplementary material related to this article can be found online at http://dx.doi.org/10.1016/j.bios.2014.05.054.

We assessed the effectiveness of the device by measuring the recovery rate of cancer cells and the removal efficiency of blood cells, both of which were evaluated based on the cells enumerated in the eluants collected after deactivating the electrodes. The recovery rate was represented by the viable portion of the cancer cells that were successfully eluted with respect to the total amount initially spiked into the samples. The average viability of the cancer cells eluted from the device was determined to be 94.05±2.91% (n=5). The removal efficiency was deduced from the enumerated blood cells in the final eluants. A low blood-cell count in the eluant thus implied that the enriched cancer cells were highly pure and suggested that blood cells were removed with high efficiency.

Fig. 4 presents the values obtained in plots as a function of the test frequency. Maximal recovery was observed using 100 kHz, with the average being 81.85±8.22%, 79.24±12.56%, and 66.94±7.37% (n=5) at flow rates of 0.1, 0.2, and 0.3 mL/h, respectively. Recovery declined as the activation approached the crossover frequency of cancer cells, at which point the pDEP forces
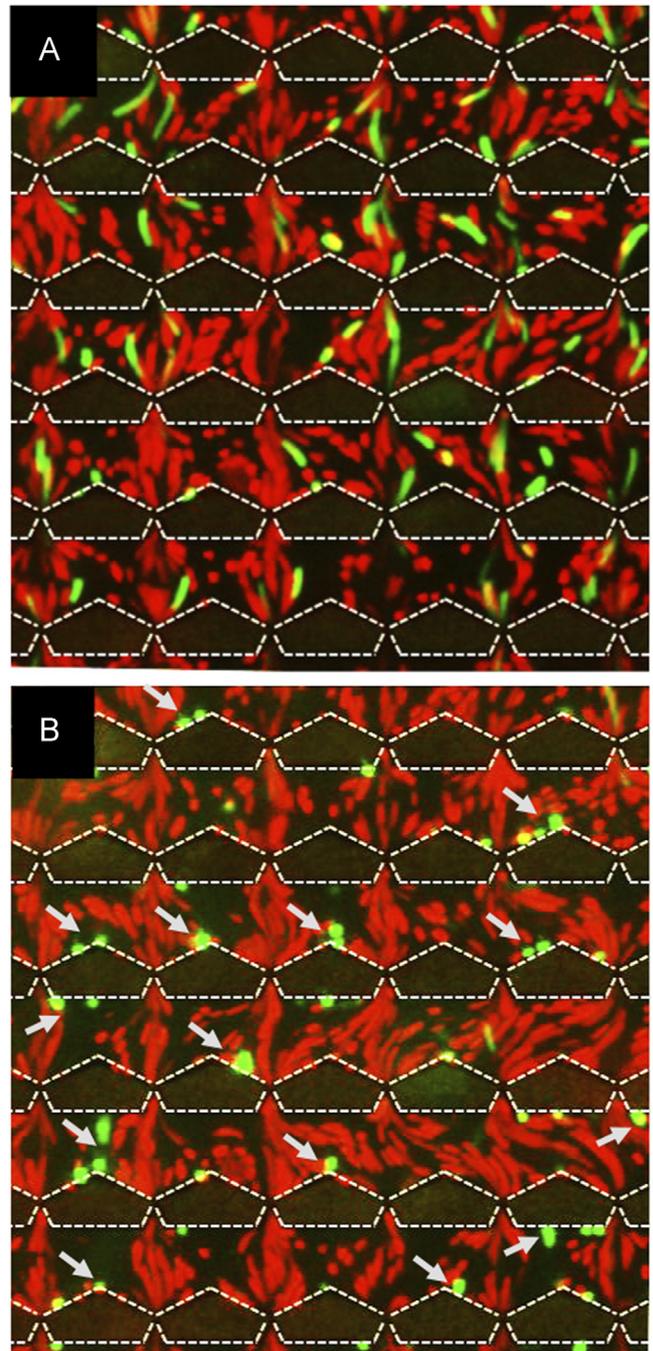
Fig. 3. A representative area of the device housing a 6-by-6 ring array (the rings between the electrode segments outlined by the dashed lines) undergoing a test: a mixture of HCT116 cells (green) and lymphocytes (red) in a DEP suspension buffer of a conductivity of 100 μS/cm was pressure injected (from top to bottom) at a flow rate of 0.2 mL/h; the images shown are from (A) before and (B) during electrode activation at ±10V_p 100 kHz. The arrows in (B) indicate some of the tumor cells that were trapped by the activated electrodes under pDEP. Although the lymphocytes were under a weak pDEP, they appear to be unaffected by the field because of the overwhelming drag force (as also shown in the movie in Supplementary Information). (For interpretation of the references to color in this figure legend, the reader is referred to the web version of this article.)

began to fade (Fig. 4A). However, within this frequency range, increasing the residence time of cells resulted in the generation of a sufficient trapping force and thus recovery improved noticeably, although a large variation was observed at the lowest flow rate tested (0.1 mL/h). Given an average recovery rate of ~80%, the combination of 100 kHz and 0.2 mL/h appears optimal. Recovery
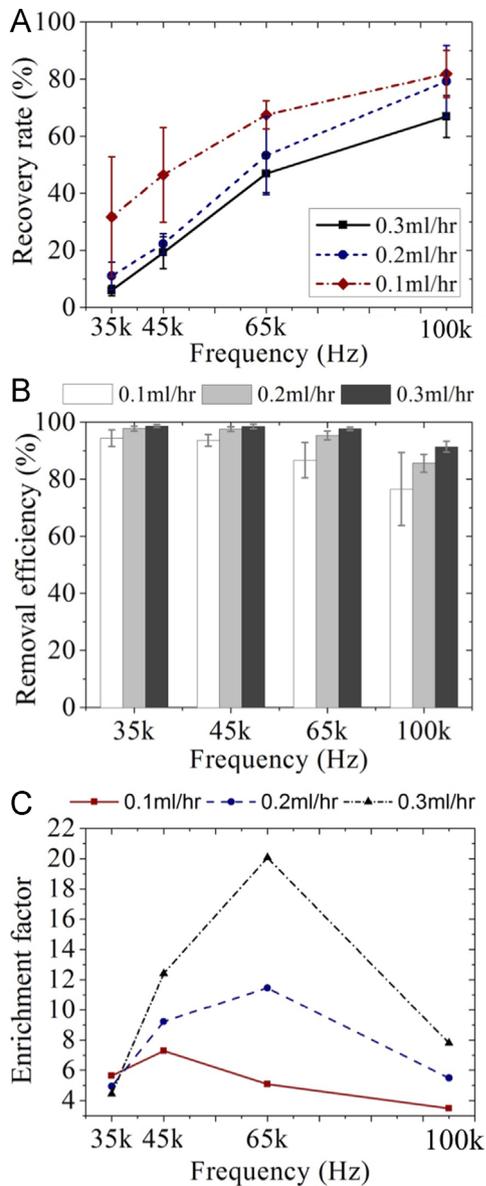
Fig. 4. (A) The rate of tumor-cell recovery, (B) the efficiency of blood-cell removal, and (C) the average cell-enrichment factor plotted against activation frequency at the 3 flow rates (see legends). The symbols and the error bars indicate the mean ± standard deviation calculated for each condition from 5 repeats performed using test samples that featured a blood-cell density of 10^7/mL and contained spiked HCT116 cells at a ratio of one tumor cell per 200 blood cells; the cells were in a suspension buffer that had a conductivity of 100 μS/cm. Each separation was performed at the stated frequency value and at a magnitude of ± $10V_p$.

called enrichment factor. The enrichment factor refers to the ratio of the cancer-cell count to the blood-cell count in the final eluent with respect to the ratio of their counts in the sample that was used as the input and processed using the device. Alternatively, this factor can be defined as the ratio of the rate of cancer-cell recovery to the fraction of the blood cells harvested together with the cancer cells (1 – efficiency of blood-cell removal). Based on this definition, the enrichment factor was calculated for each of the tested frequencies and flow rates; plotting the results against frequency (Fig. 4C) showed that a magnitude up to ~20 was registered. The maximal enrichment factor was obtained using the combination of 65 kHz and 0.3 mL/h. When the flow rate was lowered to 0.2 mL/h, the enrichment factor continued to peak around 65 kHz but was reduced by nearly 50%. This was more likely caused by the failure to efficiently remove blood cells at this reduced flow rate, because blood cells experience weak pDEP at 65 kHz, than by the inability to efficiently recover cancer cells. We noted that the average recovery rate of cancer cells was slightly higher at 0.2 mL/h than at 0.3 mL/h, at which flow rate the cancer cells were enriched by a factor of ~20 but the recovery rate was low (only 46.89 ± 6.63%). Because of the same reason, the enrichment factor was probably the lowest at 0.1 mL/h even though, on average, the rate of cancer-cell recovery was high at ≤ 65 kHz. When we used the combination of 100 kHz and 0.2 mL/h, which yielded an average recovery rate of ~80% (above), the enrichment factor was > 5. Collectively, these results allude to the ambiguity involved in relying on the enrichment factor as a sole performance indicator, particularly when isolating rare cells such as CTCs, in which case any loss of target cells cannot be afforded.

To determine whether cell recovery is an effective indicator of the cancer-cell loading in the input samples, we performed separations by using samples that were spiked with varying numbers of cancer cells, ranging in cell counts from "low" (10–50) to "high" (100–1000). These separations were all performed using the combination of 100 kHz and 0.2 mL/h. The number of cancer cells recovered was plotted against the spiked number of cancer cells (not shown) and the least-squares method was applied to fit equations. Excellent linear fits (R^2 values of 0.999 and 0.998) were obtained featuring slopes of 0.70 and 0.83, which indicated consistent recovery of 70% and 83% of the cells when the cancer-cell burden was low and high, respectively. The linearity of the plots suggests that the number of the recovered cells reflects the true cancer-cell burden in the input samples. However, to determine how far this linear range extends, additional experiments must be conducted by exploring both the upper and lower limits. Our current results indicate that using this device, we were able to recover on average 7 out of 10 cancer cells, the lowest amount spiked into the samples.

To demonstrate that the device presented here is suitable for use in future investigations on putative CTCs, we present results showing that passing cells through the device did not adversely affect cell growth. The cancer cells that were recovered were cultured and propagated in parallel with cells of the control group that had not been passed through the device. Both groups of cells exhibited comparable exponential-growth profiles over 8 consecutive days after the separation, as shown by the log plots of cell count (Fig. 5A). No noticeable difference was detected between the 2 groups. The recovered cancer cells and the control cells attached to dishes and spread normally starting from Day 1 (Fig. 5B) and exhibited normal cell division on Day 4 (Fig. 5C), and all the cells displayed the characteristic morphology of typical HTC116 cells. These results strongly suggest that the device does not exert any detrimental effect on the cell growth.

Our results are on par with those obtained using other DEP-based devices designed for isolating cancer cells; however, we obtained the results presented herein at a cell-loading concentration at least an

rates could be increased by further increasing the frequency, but this would occur at the expense of the removal efficiency of blood cells and the purity of the enriched cancer cells, because amount of blood cells retained would be increased when pDEP is strengthened. Although weak pDEP forces were exerted on blood cells at 100 kHz, the removal efficiency of the cells was high (Fig. 4B), with the averages being 85.56 ± 3.07% and 91.40 ± 1.94% ($n=5$) at flow rates of 0.2 and 0.3 mL/h, respectively, and a large variation nearly down to 60% was measured at 0.1 mL/h. At ≤ 65 kHz, the removal efficiency was > 90% except when we used 65 kHz and 0.1 mL/h; in the case of this combination, removal efficiency remained above 80%. However, blood cells were repelled at 35 and 45 kHz under negative DEP, and thus the removal efficiencies exhibited less variation.

The rate of cancer-cell recovery and the efficiency of blood-cell removal can be combined into a single figure of merit, the so-

Fig. 5. Cell growth and proliferation profile over a period of 8 days compared between the 2 HTC116 groups; "experimental" and "control" indicate the cells recovered from the device and the cells that were not passed through the device, respectively. (A) Log-plot of cell counts over days. No major difference in exponential cell-proliferation rates was detected based on determining the mean cell counts (symbols). The standard deviations (error bars) mainly arise from variations in the initial cell-seeding density among 5 separate culture repeats. (B) and (C) Images of the reseeded cells representative of the 2 groups, shown on Days 1 and 4. The cell recovery was performed at $\pm 10V_p$ 100 kHz and 0.2 mL/h.

order of magnitude higher than those used previously with an array of 3D electrodes or with coplanar electrodes that extend over a spacious layout. Moon et al. (2011), who proposed the MOFF–DEP technique, reported a high enrichment factor of 162 when separating MCF-7 breast-cancer cells from red and white blood cells, but the recovery rate measured was 75.18%. Although the front inertial module of the device (MOFF) could handle 10^7 cells/mL, the cell density dropped by an order of magnitude before the sample reached the subsequent DEP module in which coplanar electrodes occupied a layout that was 7-fold larger than the design used here. Ling et al.

(2012) used a 3D field and reported a recovery rate of 82.8% when isolating human osteosarcoma (MG-63) cells from erythrocytes at a cell mixture of 1:1 and a loading density in the order of 10^5 cells/mL. An et al. (2009) used 3D asymmetric electrodes to isolate MCF-7 breast-cancer cells from normal breast cells at a maximal efficiency of 86.6%, and the average cell-loading concentration they used was in the order of 10^6 cells/mL. Notably, unlike the recovery rates measured in this study, the high cell-recovery rates reported for some of the devices used previously were determined based on enumerating cells directly on a chip following separation and did not account for

the inevitable cell losses that are incurred when attempting to harvest the cells from the device.

The device presented herein could be used for the electrical detection and enumeration of the cancer cells isolated from lymphocytes. This can be potentially achieved by measuring impedance or conductivity changes across the interdigitated microelectrodes before and after capturing cancer cells. Alternatively, an independent set of ring microelectrodes integrated in the downstream chamber can be used to enumerate cells as they flow by individually. This type of electrical counting of captured cancer cells was shown to be highly effective in a previous design, in which a pair of platinum wires facing the output channel was used to detect the released breast-cancer cells (MCF-7) as the cells passed between the electrodes (Adams et al., 2008); given this design, whole blood could be used and spiked cancer cells were captured at a high efficiency of 97% by using high-aspect-ratio microchannels that were replicated in a polymeric substrate and decorated with mAbs specific to EpCAM. Thus, in the previous method, an incubation step was required in which a proteolytic enzyme was used to release the captured cells. This step is not required when using the device presented here. However, the samples used with our device must be prepared beforehand by removing erythrocytes, because cell–cell dielectric interactions become inevitable at extremely high loading densities, and this compromises the isolation efficiency. Nevertheless, our device can be further integrated with a coarse cell-separation modality that is highly suitable for rapidly removing erythrocytes (Moon et al., 2011).

5. Conclusions

We have demonstrated DEP-based isolation of human colorectal-carcinoma cells from blood lymphocytes by using a device whose unique design features interdigitated 3D ring array microelectrodes. Unlike traditional designs in which planar thin-film electrodes line the flow chamber, the design introduced here presents a self-aligned built-in flow chamber that is formed by the electrodes; this cultivates a highly influential DEP force field. The rings, which are designed to be comparable in size to nucleated blood cells, allow samples to sieve through while being influenced by the field at a resolution of single cells or a few cells near the rings. Because the rings are arranged in parallel, the design allows nucleated cells to be passed through at a high loading density ($\sim 10^7$ cells/mL) and yet achieves a rate of cancer-cell recovery ($\sim$82%) and an efficiency of blood-cell removal (99%) that are comparable to values reported previously using DEP-based devices. The design of our device could be further improved to ensure maximal cell recovery and purity by increasing the number of electrode digits per unit area and reducing the ineffective interspace between them. Furthermore, the ring size and locations could also be optimized. The rings here are coaxially aligned across the digits, and it would be of interest to determine how a small offset introduced into the digit-to-digit alignment, as in a deterministic bump array (Davis et al., 2006; Huang et al., 2004), affects the overall performance of the device. Lastly, we have shown that the cancer cells recovered from the device remained mostly viable (94%) and exhibited normal cell morphology and proliferation. This can be attributed at least in part to the ability of the device to dissipate heat rapidly and thus maintain the viability of captured cells. The highly efficient thermal conductance established by the 3D silicon electrodes and their large sample contact area allows the electrode digits to function as an effective heat sink, and this design ensures that a considerably lower chamber temperature is maintained as compared with the temperatures maintained using classical designs featuring thin-film planar electrodes (Tay et al., 2007).

Appendix A. Supplementary information

Supplementary data associated with this article can be found in the online version at http://dx.doi.org/10.1016/j.bios.2014.05.054.

References

Adams, A.A., Okagbare, P.I., Feng, J., Hupert, M.L., Patterson, D., Gottert, J., McCarley, R.L., Nikitopoulos, D., Murphy, M.C., Soper, S.A., 2008. J. Am. Chem. Soc. 130 (27), 8633–8641.
Alazzam, A., Stiharu, I., Bhat, R., Meguerditchian, A.N., 2011. Electrophoresis 32 (11), 1327–1336.
Alshareef, M., Metrakos, N., Juarez Perez, E., Azer, F., Yang, F., Yang, X., Wang, G., 2013. Biomicrofluidics 7 (1), 11803.
An, J., Lee, J., Lee, S.H., Park, J., Kim, B., 2009. Anal. Bioanal. Chem. 394 (3), 801–809.
Arya, S.K., Lim, B., Rahman, A.R., 2013. Lab Chip 13 (11), 1995–2027.
Becker, F.F., Wang, X.B., Huang, Y., Pethig, R., Vykoukal, J., Gascoyne, P.R., 1995. Proc. Natl. Acad. Sci. USA 92 (3), 860–864.
Becker, F.F., Wang, X.B., Huang, Y., Pethig, R., Vykoukal, J., Gascoyne, P.R.C., 1994. J. Phys. D: Appl. Phys. 27 (12), 2659–2662.
Broche, L.M., Bhadal, N., Lewis, M.P., Porter, S., Hughes, M.P., Labeed, F.H., 2007. Oral Oncol. 43 (2), 199–203.
Cen, E.G., Dalton, C., Li, Y., Adamia, S., Pilarski, L.M., Kaler, K.V., 2004. J. Microbiol. Methods 58 (3), 387–401.
Chen, J., Li, J., Sun, Y., 2012. Lab Chip 12 (10), 1753–1767.
Cheng, J., Sheldon, E.L., Wu, L., Heller, M.J., O'Connell, J.P., 1998. Anal. Chem. 70 (11), 2321–2326.
Cristofanilli, M., Budd, G.T., Ellis, M.J., Stopeck, A., Matera, J., Miller, M.C., Reuben, J.M., Doyle, G.V., Allard, W.J., Terstappen, L.W., Hayes, D.F., 2004. N. Engl. J. Med. 351 (8), 781–791.
Cristofanilli, M., Krishnamurthy, S., Das, C.M., Reuben, J.M., Spohn, W., Noshari, J., Becker, F., Gascoyne, P.R., 2008. J. Sep. Sci. 31 (21), 3732–3739.
Das, C.M., Becker, F., Vernon, S., Noshari, J., Joyce, C., Gascoyne, P.R., 2005. Anal. Chem. 77 (9), 2708–2719.
Davis, J.A., Inglis, D.W., Morton, K.J., Lawrence, D.A., Huang, L.R., Chou, S.Y., Sturm, J.C., Austin, R.H., 2006. Proc. Natl. Acad. Sci. USA 103 (40), 14779–14784.
Gascoyne, P.R., Noshari, J., Anderson, T.J., Becker, F.F., 2009. Electrophoresis 30 (8), 1388–1398.
Gascoyne, P.R., Wang, X.B., Huang, Y., Becker, F.F., 1997. IEEE Trans. Ind. Appl. 33 (3), 670–678.
Gascoyne, P.R.C., Ying, H., Pethig, R., Vykoukal, J., Becker, F.F., 1992. Measur. Sci. Technol. 3 (5), 439–445.
Gupta, G.P., Massague, J., 2006. Cell 127 (4), 679–695.
Gupta, V., Jafferji, I., Garza, M., Melnikova, V.O., Hasegawa, D.K., Pethig, R., Davis, D.W., 2012. Biomicrofluidics 6 (2), 24133.
Huang, L.R., Cox, E.C., Austin, R.H., Sturm, J.C., 2004. Science 304 (5673), 987–990.
Huang, Y., Joo, S., Duhon, M., Heller, M., Wallace, B., Xu, X., 2002. Anal. Chem. 74 (14), 3362–3371.
Huang, Y., Wang, X.B., Becker, F.F., Gascoyne, P.R., 1997. Biophys. J. 73 (2), 1118–1129.
Huang, Y., Yang, J., Wang, X.B., Becker, F.F., Gascoyne, P.R., 1999. J. Hematother. Stem Cell Res. 8 (5), 481–490.
Hyun, K.A., Jung, H.I., 2013. Electrophoresis 34 (7), 1028–1041.
Jen, C.P., Chang, H.H., 2011. Biomicrofluidics 5 (3), 34101-1–34101-10.
Jung, J., Seo, S.-K., Joo, Y.-D., Han, K.-H., 2011. Sens. Actuators B: Chem. 157 (1), 314–320.
Kang, Y., Li, D., Kalams, S.A., Eid, J.E., 2008. Biomed. Microdevices 10 (2), 243–249.
Kirby, B.J., 2010. Micro- and Nanoscale Fluid Mechanics: Transport in Microfluidic Devices. Cambridge University Press, New York.
Kostner, S., van den Driesche, S., Witarski, W., Pastorekova, S., Vellekoop, M.J., 2010. IEEE Sens. J. 10 (9), 1440–1446.
Ling, S.H., Lam, Y.C., Chian, K.S., 2012. Anal. Chem. 84 (15), 6463–6470.
Markx, G.H., Rousselet, J., Pethig, R., 1997. J. Liq. Chromatogr. Relat. Technol. 20 (16–17), 2857–2872.
Moon, H.S., Kwon, K., Kim, S.I., Han, H., Sohn, J., Lee, S., Jung, H.I., 2011. Lab Chip 11 (6), 1118–1125.
Nagrath, S., Sequist, L.V., Maheswaran, S., Bell, D.W., Irimia, D., Ulkus, L., Smith, M.R., Kwak, E.L., Digumarthy, S., Muzikansky, A., Ryan, P., Balis, U.J., Tompkins, R.G., Haber, D.A., Toner, M., 2007. Nature 450 (7173), 1235–1239.
Park, J., Kim, B., Choi, S.K., Hong, S., Lee, S.H., Lee, K.I., 2005. Lab Chip 5 (11), 1264–1270.
Rosenberg, R., Gertler, R., Friederichs, J., Fuehrer, K., Dahm, M., Phelps, R., Thorban, S., Nekarda, H., Siewert, J.R., 2002. Cytometry 49 (4), 150–158.

Sabuncu, A.C., Liu, J.A., Beebe, S.J., Beskok, A., 2010. Biomicrofluidics 4 (2), 021101.

Salmanzadeh, A., Kittur, H., Sano, M.B., C. Roberts, P., Schmelz, E.M., Davalos, R.V., 2012a. Biomicrofluidics 6 (2), 24104-1–24104-13.

Salmanzadeh, A., Romero, L., Shafiee, H., Gallo-Villanueva, R.C., Stremler, M.A., Cramer, S.D., Davalos, R.V., 2012b. Lab Chip 12 (1), 182–189.

Shim, S., Stemke-Hale, K., Noshari, J., Becker, F.F., Gascoyne, P.R., 2013a. Biomicrofluidics 7 (1), 11808.

Shim, S., Stemke-Hale, K., Tsimberidou, A.M., Noshari, J., Anderson, T.E., Gascoyne, P.R., 2013b. Biomicrofluidics 7 (1), 11807.

Steeg, P.S., 2006. Nat. Med. 12 (8), 895–904.

Sun, J.S., Gao, Y.D., Isaacs, R.J., Boelte, K.C., Lin, P.C., Boczko, E.M., Li, D.Y., 2012. Anal. Chem. 84 (4), 2017–2024.

Tan, S.J., Lakshmi, R.L., Chen, P., Lim, W.T., Yobas, L., Lim, C.T., 2010. Biosens. Bioelectron. 26 (4), 1701–1705.

Tan, S.J., Yobas, L., Lee, G.Y., Ong, C.N., Lim, C.T., 2009. Biomed. Microdevices 11 (4), 883–892.

Tay, F.E.H., Yu, L.M., Pang, A.J., Iliescu, C., 2007. Electrochim. Acta 52 (8), 2862–2868.

Thiery, J.P., Sleeman, J.P., 2006. Nat. Rev.: Mol. Cell Biol. 7 (2), 131–142.

Valero, A., Braschler, T., Renaud, P., 2010. Lab Chip 10 (17), 2216–2225.

van den Driesche, S., Rao, V., Puchberger-Enengl, D., Witarski, W., Vellekoop, M.J., 2012. Sens. Actuators B: Chem. 170 (0), 207–214.

Vona, G., Sabile, A., Louha, M., Sitruk, V., Romana, S., Schutze, K., Capron, F., Franco, D., Pazzagli, M., Vekemans, M., Lacour, B., Brechot, C., Paterlini-Brechot, P., 2000. Am. J. Pathol. 156 (1), 57–63.

Wang, X.B., Yang, J., Huang, Y., Vykoukal, J., Becker, F.F., Gascoyne, P.R., 2000. Anal. Chem. 72 (4), 832–839.

Wong, L.S., Bateman, W.J., Morris, A.G., Fraser, I.A., 1995. Br. J. Surg. 82 (10), 1333–1337.

Xing, X.X., Zhang, M.Y., Yobas, L., 2013. J. Microelectromech. Syst. 22 (2), 363–371.

Yang, F., Yang, X., Jiang, H., Bulkhaults, P., Wood, P., Hrushesky, W., Wang, G., 2010. Biomicrofluidics 4 (1), 13204.

Yang, J., Huang, Y., Wang, X.B., Becker, F.F., Gascoyne, P.R., 1999. Anal Chem 71 (5), 911–918.

Yobas, L., Sharma, R.K., Nagarajan, R., Samper, V.D., Naidu, P.S.R., 2005. J. Micromech. Microeng. 15 (2), 386–393.

Zhu, J., Xuan, X., 2011. Biomicrofluidics 5 (2), 24111.